Korean J. Chem. Eng., 33(4), 1447-1455 (2016)
DOI: 10.1007/s11814-015-0280-y

pISSN: 0256-1115
eISSN: 1975-7220

Electrochemical performance of three shaped ZnO nanoparticles prepared in LiOH, NaOH and KOH alkaline solutions as anodic materials for Ni/Zn redox batteries

Younghwan Im*, Sora Kang*, Byeong Sub Kwak*, Kyoung Soo Park, Tae Woo Cho**, Jin-Sik Lee**, and Misook Kang*,†**

*Department of Chemistry, College of Science, Yeungnam University, Gyeongsan, Gyeongbuk 38541, Korea
**Research & Development Center, Vitzrocell Co., Yesan-gun, Chungnam 23535, Korea
(*Received 27 August 2015 • accepted 11 December 2015*)

Abstract−ZnO nanoparticles with three morphologies were synthesized by a hydrothermal route at 120 °C for 3 h in high alkaline aqueous solutions of LiOH, NaOH, and KOH. We analyzed them by X-ray diffraction (XRD), scanning electron microscopy/energy dispersive spectroscopy (SEM/EDS), cyclic voltammetry (CV), Zeta potential measurement, and impedance. XRD and SEM showed that the obtained ZnO nanoparticles had high purity and perfect crystallinity, and the morphologies of the particles prepared in the LiOH, NaOH, and KOH solutions showed nanoplate, nanobead, and nanorod shapes, respectively. CV showed that the nanoplate ZnO-LiOH and nanorod ZnO-KOH have superior electrochemical activity to that of the other ZnO nanostructures. As electrode materials of Ni/Zn redox batteries, the nanoplate ZnO-LiOH showed a significantly improved cycle stability after the 30^{th} cycle compared to that of ZnO-NaOH and conventional ZnO with a mean discharge capacity of 153 mA h g^{-1}, a cell efficiency of 93%, and higher discharge voltages of 1.9. In addition, during the charging/discharging cycles, the growth of zinc dendrite clusters could be suppressed, which resulted in an improvement in the cycle stability of the Ni/nanoplate ZnO-LiOH redox cell.

Keywords: Ni/Zn Redox Battery, ZnO Nanoparticles, Charge/Discharge, Zinc Dendrite Clusters

INTRODUCTION

Since the redox flow battery (RFB) concept was first proposed by Thaller [1] in 1974, many types of redox flow batteries have been fabricated [2-5]. The Ni/Zn redox battery has high specific energy, high specific power, high open-circuit voltage, low toxicity, and low cost. In particular, the free-membrane alkaline zinc-nickel redox battery has a nominal voltage of 1.6 V (theoretical value 1.72 V) per cell [6,7], and it has an almost constant voltage during most of the discharge period, exhibiting voltage stability at different discharge rates. In addition, the raw materials for zinc/nickel batteries are abundant and environmentally friendly. However, the widespread commercialization of this kind of Zn-based battery has been limited by its low cycling life. The major problems with rechargeable Ni/Zn batteries are the shape change of the electrode, dendrite growth, passivation, and self-discharge of the Zn electrodes [8-10]. In particular, the short cycle life of the zinc anode arises mainly from dendritic growth (in the anode, zincate anions $Zn(OH)_4^{-2} \rightarrow ZnO+H_2O+2OH^-$) [11]. Many attempts have made to suppress ZnO dendritic growth, including some additives to the zinc electrode (e.g., Ca, Bi, Ag, C, Mn, and Al) [12-17]. Two aspects of ZnO electrode materials should be given careful consideration for size and morphology [18,19]. In particular, the problems of Ni/Zn secondary batteries are strongly related to the physical and electrochemical properties of ZnO. The initial morphology of ZnO can influence the electrochemical performance of secondary Ni/Zn batteries [19]. Wen et al. reported [20] the electrochemical performance of ZnO with different morphologies, hollow fusiform ZnO and hexagonal taper-like ZnO, as the anodic materials for Ni/Zn secondary batteries. They concluded that hollow fusiform ZnO and hexagonal taper-like ZnO showed better cycle stability than conventional ZnO, and the formation of zinc dendrites was suppressed considerably. This was attributed to the initial morphology of the anodic materials. Yang et al. [21], through low rate cyclic voltammetry, showed that the electrochemical performance of ZnO nanowires was superior to that of conventional ZnO. Ma et al. [19] also evaluated the electrochemical performance of the ZnO nanoplates, and reported its better cycle stability than the conventional ZnO with a discharge capacity maintained at 420 mA h g^{-1} throughout 80 cycling tests.

However, little attention has been focused on the effects of the different morphologies of ZnO on the electrochemical properties. The shape change and dendrite growth are possibly related to the morphology of the anodic active material. To further illustrate this point, it is very important to examine the electrochemical performance of ZnO with different morphologies. In the present work, nanoplates-, threaded nanobeads-, and nanorods-shaped ZnO particles are prepared via hydrothermal method. As the anodic active materials for the free membrane alkaline Zn/Ni redox battery, their electrochemical properties are examined in detail.

MATERIALS AND METHODS

1. Preparation and Characterization of the ZnO Powders

The ZnO powers were prepared using a hydrothermal route. Briefly, the appropriate amount of the zinc nitrate ($Zn(NO_3)_2$ xH_2O,

†To whom correspondence should be addressed.
E-mail: mskang@ynu.ac.kr

99.99%, Aldrich) precursors to produce a 1.0 M solution were dissolved in 1.0 L of a water/ethanol mixed solution in three separate beakers with stirring. Subsequently, 2.0 M-LiOH (LiOH H_2O, 99.95%, Aldrich), -NaOH (99.99%, Aldrich), and -KOH (99.99%, Aldrich) were added to the three beakers to produce three mixtures. After being stirred for 3 h, the solutions were transferred to three autoclaves for the thermal treatment. The temperatures of the autoclaves were increased with 10 °Cmin^{-1} to 120 °C, and kept there for 3 h with the natural vapor pressure of ethanol. After the thermal treatment, the final precipitates were filtered, washed several times with distilled water to pH 7.0, and dried at 70 °C for 24 h. The expected synthesis mechanisms of the ZnO powers are as follows:

1) $Zn(NO_3)_2$+2LiOH (NaOH or KOH)
$\rightarrow 2Li^+$ (Na^+ or K^+)+$2NO_3^-$+$Zn(OH)_2$
2) $Zn(OH)_2 \rightarrow ZnO+H_2O$

The synthesized ZnO powders were called conventional ZnO, ZnO-LiOH, ZnO-NaOH, and ZnO-KOH according to the alkaline additives used, and they were examined by X-ray diffraction (XRD, MPD, PANalytical) using nickel-filtered CuKα radiation (30 kV, 30 mA). Scanning electron microscopy (SEM, JEOL 2000EX) at acceleration voltages of 120 and 200 kV was performed to determine the particle sizes and morphologies of the materials. The atomic compositions in ZnO powders were measured by energy dispersive X-ray spectroscopy (EDS, EX-250, Horiba) operated at 120 kV. The zeta potentials of the ZnO powders were determined from the electrophoretic mobility using an electrophoresis measurement apparatus (ELS 8000, Otsuka Electronics, Japan). Electrophoretic light scattering (ELS) was performed in reference beam mode using a laser light source of 670 nm, a modular frequency of 250 Hz and a scattering angle of 15°. The standard error of the zeta potential, which had been converted from the experimentally determined electrophoretic mobility, was typically <1.5% and the percentage error was <5%. To measure the zeta potential, 0.1 wt% of each sample was dispersed in de-ionized water and the pH of the solution was adjusted using HCl or NaOH. The relative molecular diameter size distributions of the various pH solutions were also measured using this equipment.

2. Electrochemical Performance of the ZnO Anodic Materials in a Ni/Zn Cell

The galvanostatic charge-discharge tests were performed using a battery test system, WPG100e (WonA Tech., Korea) at room temperature (25±2 °C) using a small single stationary vial-type cell, similar to that in a previous study [22]. Before the cycling test, the cells were pre-charged at 5 mA cm^{-2} for 10 h and pre-discharged at 10 mA cm^{-2} down to the 1.4 V cut-off to stabilize the oxidation-reduction state of active species in the cell. During the cycling procedure, the cells were charged at a current density of 20 mA cm^{-2} for 1.5 h and discharged at 20 mA cm^{-2} to the 1.4 V cut-off. Two electrodes, a sintered NiOOH foam (0.7 mm in thickness, loaded Ni amount 180.0 mg cm^{-2}) as the cathode and a 0.1 mm thick nickel plate as the anode, were placed on both sides. The cathode and anode electrodes were 1.0 cm×1.0 cm (width×height), and the distance between them was maintained at 1.0 cm. The cell compartment was filled with 10 mL of a 0.5 M ZnO anodic material in an 8 M KOH aqueous solution. The electrochemical oxidation-reduction reaction in the cell is as follows:

Positive: $2NiOOH+2H_2O+2e^- \rightarrow 2Ni(OH)_2+2OH^-$
Negative: $Zn+4OH^- \rightarrow Zn(OH)_4^{2-}+2e^-$
Overall: $Zn+2OH^-+2H_2O+2NiOOH \rightarrow 2Ni(OH)_2+Zn(OH)_4^{2-}$

CV was also performed using the same galvanostatic scanning rate of 50 mV s^{-1} from −1.0 V to −2.0 V at room temperature (25± 1 °C). The electrolyte was 0.5 M ZnO in 8 M KOH solution. A three-electrode cell assembly was used in the test. Ag/AgCl electrode served as reference. The working electrode was a Ni-plate, and the Pt electrode was used as the counter electrode. The sizes are the same as that of the electrode which was used in the charge-discharging test, 0.5 cm×0.5 cm (width×height).

RESULTS AND DISCUSSION

1. Physical Properties of the Synthesized ZnO Powders

Fig. 1 shows XRD patterns of the conventional ZnO and ZnO powders, which were prepared using a hydrothermal method. All the XRD peaks were indexed to the hexagonal wurtzite ZnO [space group P63mc] with lattice constants of a=3.251 Å and c=5.212 Å, according to JCPDS file No. 36-1451 [23], and no other impurity peaks were observed. The XRD peaks could be classified into the following three groups: pyramidal planes of (101), (102), (103), (112), and (201); prismatic planes of (100), (110) and (200); and polar plane of (002). The strong and widened diffraction peaks indicate that the material has perfect crystallinity and a very small particle size. The pattern showed very sharp peaks, indicating that conventional ZnO and ZnO-LiOH have good crystallization; however, the peak intensities in the ZnO-NaOH and ZnO-KOH particles were relatively weak. Peak broadening indicated a decrease in crystallite size. The full widths at half maximum (FWHM) of the 31.7° 2θ (100) peaks in the four ZnO samples were measured: the crystallite sizes of the conventional ZnO, ZnO-LiOH, ZnO-NaOH, and ZnO-KOH estimated using the Debye-Scherrer equation [24] were 35, 27, 25, and 30 nm, respectively.

Fig. 2 presents SEM images of the conventional ZnO and ZnO

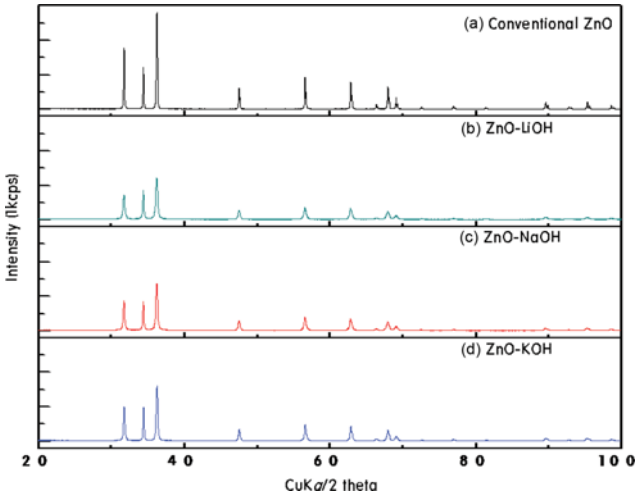

Fig. 1. XRD patterns of the conventional ZnO and ZnO powders prepared by hydrothermal synthesis.

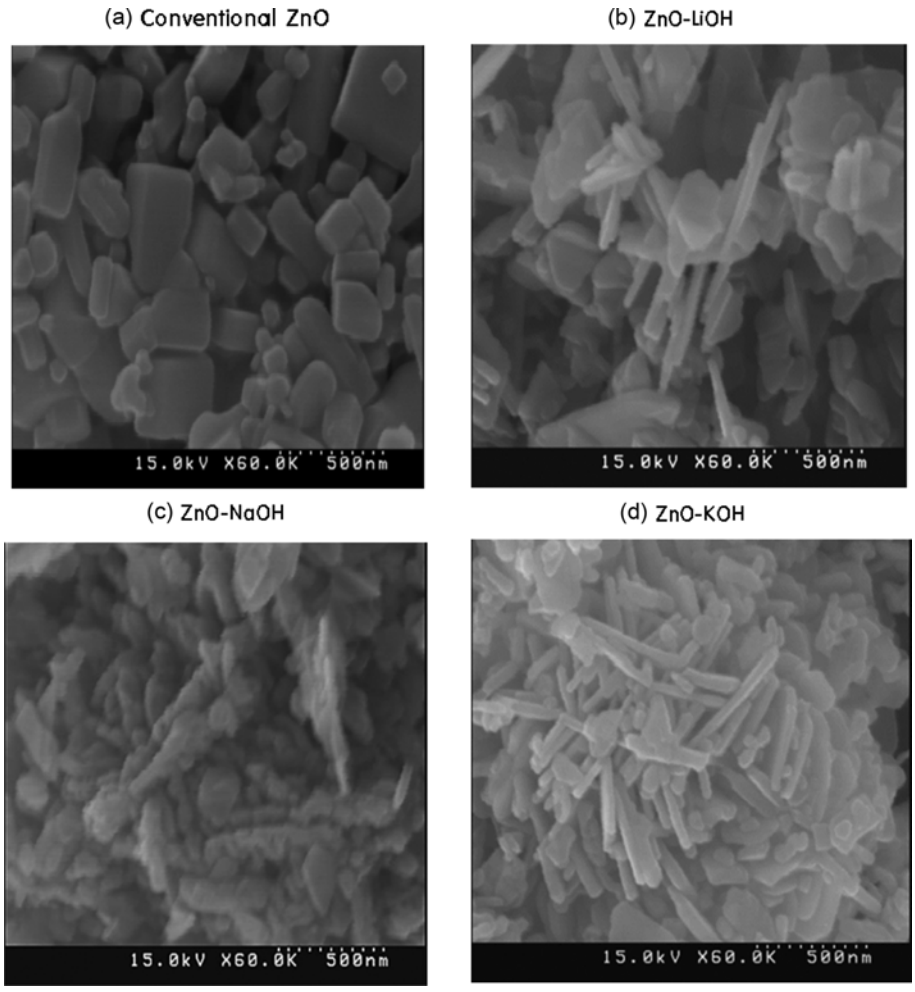

Fig. 2. SEM images of the conventional ZnO and ZnO powders prepared by hydrothermal synthesis.

powders prepared by the hydrothermal method, which indicates some novel micro- and nanostructures. The conventional ZnO particles mainly have the typical cubic shapes with sizes of approximately 100-500 nm, as shown in Fig. 2(a). The nanoplates, 300 nm in length, 250 nm in width and 50 nm in height, were clearly observed in the ZnO particles prepared in the LiOH solution (Fig. 2(b)). The product was observed as an irregular pyramid with a wide range of dimensions. Otherwise, the threaded nanobeads and nanorods, approximately 500 nm in length, which assembled of some sub-spindles and sub-pillars of ZnO crystals, were observed in the ZnO-NaOH and ZnO-KOH particles shown in Fig. 2(c) and (d), respectively. The difference of morphology can be explained by Pearson's hard soft acid base rule that hard acids prefer hard bases. The hard intensity in acid was decreased in the order of Li> Na>K, and the OH^- is a hard base. Therefore, in the synthesis step of ZnO, the Zn hydrolysis in KOH solution is faster than that of other basic solutions. Therefore, the crystal growth rate of ZnO is also increased in KOH solution (rod type). Then the next order is to be NaOH and LiOH, respectively; they show the threaded nanobead- and nanoplate-shaped morphologies.

Fig. 3 shows the influence of pH on the position of the zeta potential distribution median (determined using electronic light scattering) of the ZnO powders. In all samples, the surface charge changed from a positive value in an acidic solution to a negative value in an alkali solution. The isoelectric point (ip) was pH 7.4 in conventional ZnO with significant aggregation. In contrast, the

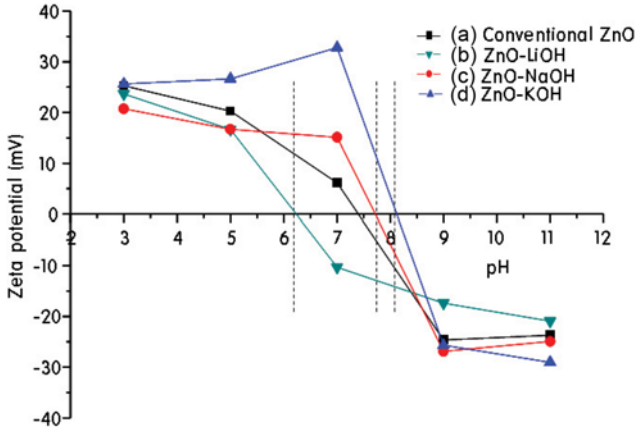

Fig. 3. Zeta potential distributions depending on the influence of the pH of the ZnO powders.

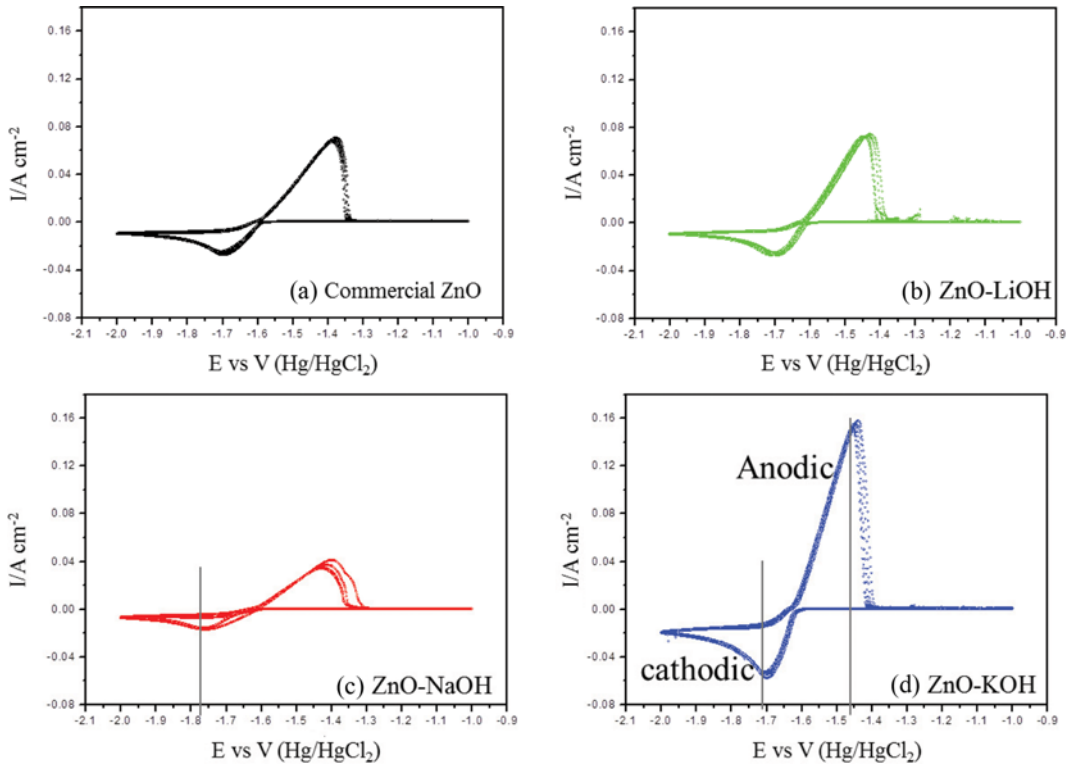

Fig. 4. Cyclic voltammetry curves of the conventional ZnO and ZnO powders.

point shifted to a higher pH in the nanobead ZnO-NaOH and nanorod ZnO-KOH suspensions around the ip; pH 7.7 and 8.2, respectively. In addition, the surface charges had the highest values in a basic solution, which generally means stable particles [25]. On the other hand, the ip was rather shifted to a lower pH in the nanoplate ZnO-LiOH suspensions, but the highest absolute value also increased in the alkaline solution. This suggests that the ZnO colloids are more stable in alkali solutions with little aggregation; hence, the redox reaction will progress more easily in an alkaline solution than in an acidic solution.

To further investigate the influence of ZnO morphology on electrochemical reactions, cyclic voltammograms (CV) for ZnO-LiOH, ZnO-NaOH, ZnO-KOH, and commercial ZnO were conducted, and the CV curves for 10^{th}, 20^{th}, 30^{th}, 40^{th}, and 50^{th} cycles are presented in Fig. 4. The cathodic peaks containing the conventional ZnO, the ZnO-LiOH, ZnO-NaOH, and ZnO-KOH, appeared at −1.50, −1.50, −1.50, and −1.51 V against NHE, respectively, which are associated with the reduction of Zn(II) ions to Zn(0). Compared with ZnO-LiOH and ZnO-KOH show a much higher peak current, suggesting that the reduction of these two zinc electrodes is favorably enhanced. The cathodic peaks of ZnO-LiOH and ZnO-KOH were much steeper than those of conventional ZnO and ZnO-NaOH. The cathodic peak is in accord with the charging process of a secondary battery. This characteristic of cathode peak demonstrates that the ZnO-LiOH and ZnO-KOH have rapid reduction reaction kinetics, and the charging process is more effective and rapid. In particular for ZnO-KOH, a more negative potential, generally speaking, means a lower electrochemical kinetics of reduction process. Otherwise, when the potential scan is switched to the positive direction, the anodic peaks, which were different from three negative electrodes, appeared at about −1.24, −1.22, and −1.25 V against NHE for the ZnO-LiOH, ZnO-NaOH, and ZnO-KOH, respectively, which were shifted in the more negative direction in comparison with the conventional ZnO (−1.17 V). These phenomena manifested that the reversibility of the reaction became obviously better in this system. The anodic process is corresponding to the discharge process of the zinc electrode. The increase of the anodic peak is in accord with the higher discharge voltage. The areas of anode peak of ZnO-LiOH and ZnO-KOH were also larger than that of the conventional ZnO, which results from the higher electrochemical activity.

2. Electrochemical Performance of the ZnO Anodic Materials in a Ni/Zn Cell

Fig. 5 shows the typical galvanostatic charge-discharge voltage (V) curves versus current time (min) with increasing numbers of cycles from the 1^{st} to 30^{th}-cycles at 20 mA cm^{-2} for a 1.5 h charge-discharge of the ZnO anodic materials in the Ni/Zn electronic chemical system. With the exception of nanobead ZnO-NaOH, the charge-discharge curves of the other samples were similar. For the nanobead ZnO-NaOH, the dramatically higher charge and lower discharge plateau voltages with increasing number of cycles possibly induced an increase in H_2 formation [27], resulting in a lower discharge plateau, i.e., lower output energy and power. Moreover, the efficiency declined rapidly with increasing numbers of cycles compared to the other samples. Otherwise, the morphologies of the nanoplate and nanorod in the ZnO particles were compared favorably with the conventional ZnO in terms of the charge plateau voltage, discharge plateau voltage and discharge capacity. Furthermore, the high

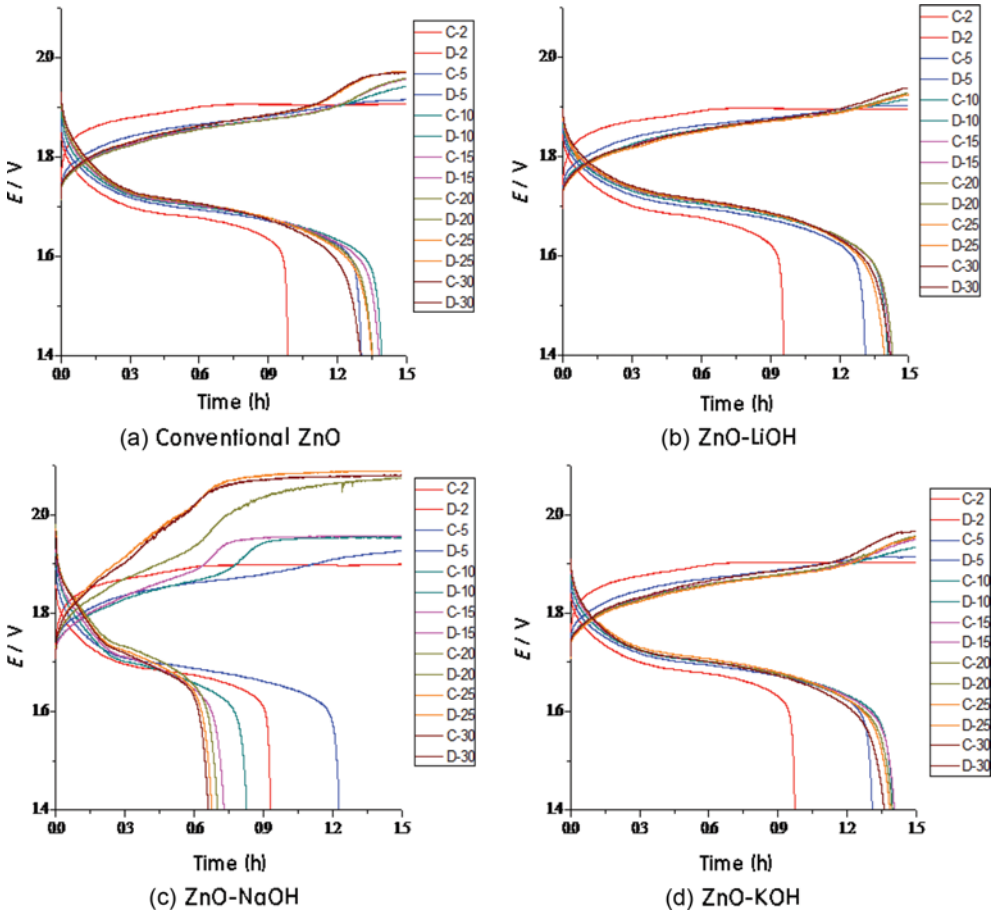

Fig. 5. Typical galvanostatic charge-discharge voltage curves versus the current time with an increase in the number of cycle numbers for the ZnO anodic materials in the Ni/Zn redox cell.

efficiencies were continued stably to the 30th cycles. The charge midpoint voltage of the nanoplate ZnO-LiOH for the 30th-cycle was 0.02 V, lower than that of the conventional ZnO, and the discharge midpoint voltage was 0.03 V, higher than that of the conventional ZnO. In particular, for the nanoplate ZnO-LiOH, the low charge plateau voltage was conducted for the suppression of H_2 formation and increase in charge efficiency, which possibly resulted in a high output energy and power. The lower charge voltage, higher discharge voltage and higher discharge capacity are the most convincing evidence for excellent electrochemical perfor-

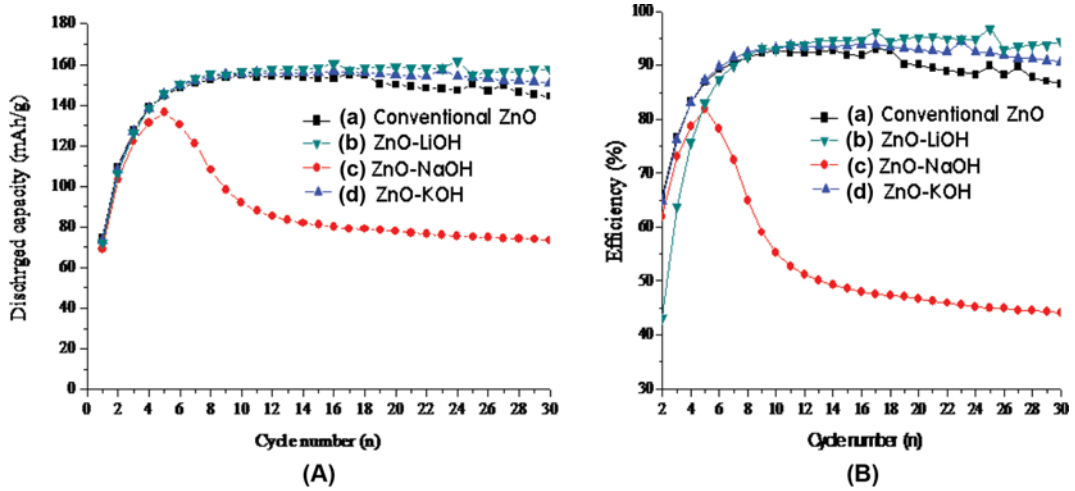

Fig. 6. Electrochemical cycle behaviors of the electrodes with the conventional ZnO and ZnOs prepared in this study: (a) Discharged capacity versus cycle number and (b) efficiency versus cycle number.

mance of nanoplate ZnO-LiOH.

Fig. 6(a) and (b) present the electrochemical cycle behavior of the electrodes with the conventional ZnO and ZnOs prepared in this study. The initial (for 10th cycle) discharge capacity of the conventional ZnO was approximately 150 mA h g^{-1} with a 92% cell efficiency after activation, but it decreased slowly after several cycles with a capacity retention ratio of 84% at the 30th cycle. Compared to conventional ZnO, the initial discharge capacities and capacities retention ratio of the nanoplate ZnO-LiOH and nanorod ZnO-KOH were improved slightly, reaching approximately 155 mA h g^{-1} and 94%. The discharge capacity barely declined over the 30 cycling tests, but the efficiency of the nanorod ZnO-KOH was slightly inferior to the nanoplate ZnO-LiOH. Consequently, nanoplate ZnO-LiOH maintained a discharge capacity of 153 mA h g^{-1} with a capacity retention ratio of 93% for more than 30th cycle, which is remarkably superior to the conventional ZnO. The results show that the nanoplate ZnO-LiOH and nanorod ZnO-KOH have a higher discharge capacity and more stable electrochemical cycle performance than conventional ZnO. In contrast, in the case of nanobead ZnO-NaOH, the initial (for 7th cycle) discharge capacity was approximately 138 mA h g^{-1} with 82% efficiency after activation, but it decreased rapidly after several cycles with a capacity retention ratio of 45% at the 30th cycle. This was attributed to hydrogen generation, as illustrated in Fig. 5.

To examine the influence of the ZnO morphologies on the impedance of the pasted electrode, EIS was carried out and the impedance diagrams are presented in Fig. 7. The Nyquist plots in all samples involved a high-frequency capacitive semicircular loop and low-frequency straight line. The high-frequency capacitive semicircular loop was assigned to charge-transfer resistance in parallel

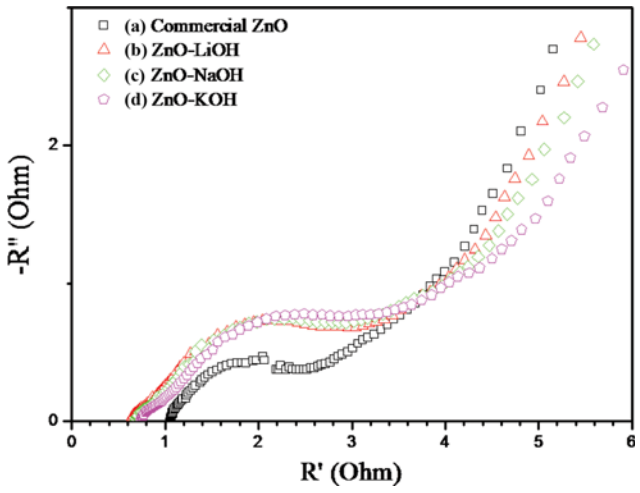

Fig. 7. Impedance diagrams determined from the EIS measurements of the electrodes with the conventional ZnO and ZnOs prepared in this study.

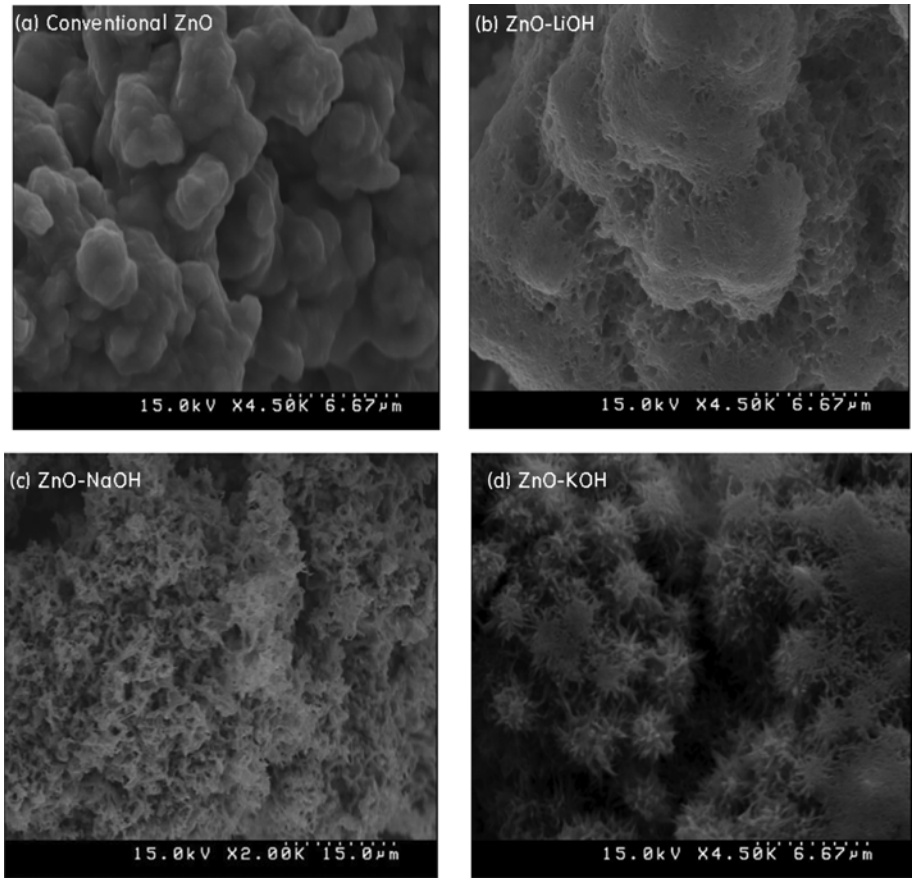

Fig. 8. SEM images of the ZnO aggregations incorporated into Ni-plate electrodes after the 30th charge-discharge cycling test.

with the double-layer capacitance, and the slope in the low-frequency region was most probably caused by the diffusion of zincate in the zinc anodic material [28]. The equivalent circuit used to fit the EIS spectra is also reported: CPE represents the constant phase element for a porous electrode; R_e is the total ohmic resistance, which includes the resistance of the electrolyte, current collector, electrode materials, etc.; R_{ct} is the charge-transfer resistance; and Z_w is the Warburg impedance [29]. According to the equivalent circuit, the fitted R_{ct} of ZnO-LiOH, ZnO-NaOH, ZnO-KOH, and the conventional ZnO electrodes were 2.93, 3.38, 3.58, and 2.85 ohms, respectively. The differences of R_{ct} values were not big depending on their morphologies in this study. A larger R_{ct} means a more difficult electrochemical reaction, which leads to an increase in electrochemical polarization. The fitted R_e for ZnO-LiOH and the conventional ZnO electrodes were smaller than those of ZnO-NaOH and ZnO-KOH. A smaller R_e generally bears the sign of better electrical conduction and weaker ohmic polarization. A factor that may partly contribute to the smaller R_e: ZnO is an n-type semiconductor, which can have a different band-gap depending on their morphologies [30]. Therefore, as an electrode material, the nanoplate ZnO-LiOH in the electrochemical reaction would decrease the resistance of the electrode.

Fig. 8 presents SEM images of the ZnO aggregations incorporated into the Ni-plate electrode after the 30th charge-discharge cycling tests. The conventional ZnO (a) and nanobead ZnO-NaOH (c) were deposited randomly on the Ni-plate electrode and the shapes in both samples were similar. Ten-micron features with the appearance of moon craters with a relatively large difference in particle sizes and many dendrite clusters were observed over the electrode surface. These cubic and round bead-like ZnO particles might be connected in the same directions as each other, and create a hole in the end to give the appearance of a moon crater. The formation of dendrite clusters was already explained by the outward texture growth of the electrodeposited growth theory [31]. The dendrites penetrate the separators readily, resulting in an interior short circuit, and a decrease in the discharge capacity of the batteries. This coincides with the reducing discharge capacity of the cubic-like conventional ZnO and nanobead ZnO-NaOH. With further increases in the charge/discharge number, the quantity of dendrite clusters increased gradually. As a result, the discharge capacity decreased gradually. In addition, some interesting nanoplate ZnO-LiOH was observed over the Ni-plate electrode, as shown in Fig. 8(b). The size of 6-micron and the shapes, such as cotton balls, were relatively uniform, resulting from the breaking of nanoplates caused by the dissolution of ZnO/Zn in the alkaline electrolyte. The surface activity of the nanoplate ZnO-LiOH was relatively high due to the size effect of the nanomaterials. Therefore, the broken nanoplate ZnO particles will perform epitaxial electrodeposited growth during the charge/discharge cycles because of the high surface activity. Consequently, the ZnO nanoplates become thicker, so the growth of Zn dendrites is suppressed and the cyclic stability of ZnO is improved. Finally, in the case of nanorod ZnO-KOH (d), the perfect zinc dendrite with a relatively small (3-micron) and sharp like a sea urchin features were shown, which indicates the sea urchin results from slowly electrodeposited growth between the nanorods step by step. This electrodeposited growth could be the inadequate growth attributed to surface passivation, resulting in a decrease in the dissolution of ZnO/Zn into the electrolyte. The (0001) plane is the fastest crystal growth direction in the hcp crystal structure of ZnO for a dendrite growth mechanism [32]. Despite growing zinc dendrites using nanorod ZnO-KOH, the electric performance was quite good in this study. The reason for this is explained in a previous report [33], which indicates that the nanorod shaped ZnO possesses excellent electrochemical cycle performance, and the nanorod does not damage the electrochemical performance of ZnO. As a result, the nanorod-shaped ZnO can show good discharge capacity and cycle stability throughout the cycling test in this study.

Fig. 9 presents the EDX spectrum of the ZnO aggregations incorporated into the Ni-plate electrode after the 30th charge-discharge

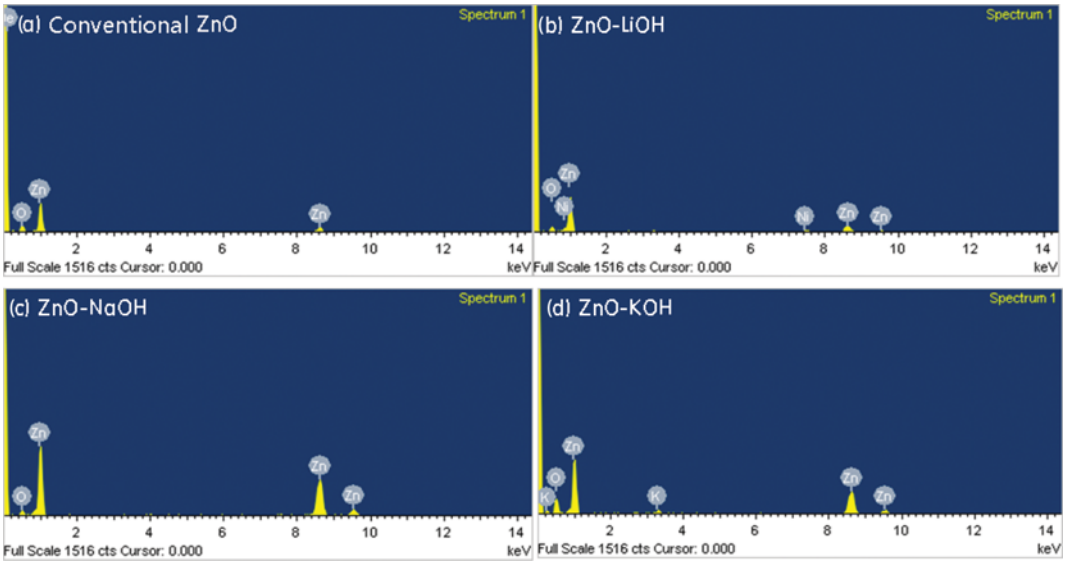

Fig. 9. EDS of the ZnO aggregations incorporated into Ni-plate electrodes after the 30th charge-discharge cycling test.

Table 1. Atomic compositions analyzed from EDS

	Conventional ZnO		ZnO-LiOH		ZnO-NaOH		ZnO-KOH	
Elements	Weight (%)	Atomic (%)	Weight (%)	Atomic (%)	Weight (%)	Atomic (%)	Weight (%)	Atomic (%)
Zn	85.77	59.59	84.44	67.45	98.33	93.50	91.87	74.94
O	14.23	40.41	7.88	25.72	1.67	6.50	7.09	23.64
K	-	-	-	-	-	-	1.04	1.42
Ni	-	-	7.68	6.83	-	-	-	-
Totals	100	100	100	100	100	100	100	100

cycling test. Only the Ni elements showed a fresh Ni-plate electrode. On the other hand, the peaks of Zn and O can be clearly found in the spectra upon the used Ni-plate electrodes after the 30^{th} charge-discharge cycling test. The peak intensity of Zn was strongest when nanobead ZnO-NaOH was used, but was smallest in nanoplate ZnO-LiOH.

Table 1 lists the atomic compositions analyzed from the EDS spectrum. The quantity of Zn deposited on the Ni-foam electrode was lower in the Ni/ZnO-LiOH redox battery than the others. The quantities of Zn deposited on the Ni-plate electrodes increased in the order of Ni/ZnO-LiOH<Ni/ZnO-KOH<Ni/Conventional ZnO< Ni/ZnO-NaOH redox battery. This confirms the control of the ZnO morphology in the Ni/Zn redox battery cell, which can eventually suppress the growth of Zn dendrites.

CONCLUSIONS

Nanoplate-, nanobead- and nanorod-ZnOs were prepared in LiOH, NaOH and KOH alkaline solutions via a hydrothermal method, which showed better discharge stability as anodic materials for Ni/Zn redox cells compared to the conventional ZnO. In particular, the narrow charge/discharge voltage range and the high discharge value are evidence of its good electrochemical performance in Ni/nanoplate ZnO-LiOH cell. This suggests that it is more suited as an anodic material for Ni/Zn redox battery than the conventional one. The maintenance of the discharge capacity was attributed to the novel initial morphology of nanoplate ZnO, making it difficult for the active material to transform to zinc dendrites during the charging and discharging process. In contrast, some irregular moon craters were observed when nanocubes and nanobeads were used. These results confirm that the initial morphology of the active materials can control and suppress the morphology of the zinc dendrite effectively, resulting in an improvement in the cycle stability of Ni/Zn redox cells.

ACKNOWLEDGEMENTS

This study was supported by the World Class 300 Project, Small and Medium Business Administration, Republic of Korea, for which the authors are very grateful.

REFERENCES

1. L. H. Thaller, NASA TM X-71540 (1974).
2. F. Chen, Q. Sun, W. Gao, J. Liu, C. Yan and Q. Liu, *J. Power Sources*, **280**, 227 (2015).
3. D. H. Hyeon, J. H. Chun, C. H. Lee, H. C. Jung and S. H. Kim, *Korean J. Chem. Eng.*, **32**, 1554 (2015).
4. S. M. Park and H. Kim, *Korean J. Chem. Eng.*, **32**, 2434 (2015).
5. G. Nikiforidis, L. Berlouis, D. Hall and D. Hodgson, *Electrochim. Acta*, **125**, 176 (2014).
6. Y. Cheng, H. Zhang, Q. Lai, X. Li, D. Shi and L. Zhang, *J. Power Sources*, **241**, 196 (2013).
7. Y. Cheng, H. Zhang, Q. Lai, X. Li, Q. Zheng, X. Xi and C. Ding, *J. Power Sources*, **249**, 435 (2014).
8. C. J. Lan, C. Y. Lee and T. S. Chin, *Electrochim. Acta*, **52**, 5407 (2007).
9. A. Nakata, H. Murayama, K. Fukuda, T. Yamane, H. Arai, T. Hirai, Y. Uchimoto, J. Yamaki and Z. Ogumi, *Electrochim. Acta*, **166**, 82 (2015).
10. H. Yang, Y. Cao, X. Ai and L. Xiao, *J. Power Sources*, **128**, 97 (2004).
11. Y. F. Yuan, L. Q. Yu, H. M. Wu, J. L. Yang, Y. B. Chen, S. Y. Guo and J. P. Tu, *Electrochim. Acta*, **56**, 4378 (2011).
12. R. Wang, Z. Yang, B. Yang, X. Fan and T. Wang, *J. Power Sources*, **246**, 313 (2014).
13. Y. F. Yuan, Y. Li, S. Tao, F. C. Ye, J. L. Yang, S. Y. Guo and J. P. Tu, *Electrochim. Acta*, **54**, 6617 (2009).
14. J. Z.Wu, J. P. Tu, Y. F. Yuan, M. Ma, X. L. Wang, L. Zhang, R. L. Li and J. Zhang, *J. Alloys Compd.*, **479**, 624 (2009).
15. B. Yang, Z. Yang, R. Wang and T. Wang, *Electrochim. Acta*, **111**, 581 (2013).
16. R. Rácz and P. Ilea, *Hydrometallurgy*, **139**, 116 (2013).
17. R. Wang, Z. Yang, B. Yang, T. Wang and Z. Chu, *J. Power Sources*, **251**, 344 (2014).
18. Y. F. Yuan, J. P. Tu1, H. M. Wu, Y. Li and D. Q. Shi, *Nanotechnol.*, **16**, 803 (2005).
19. M. Ma, J. P. Tu, Y. F. Yuan, X. L. Wang, K. F. Li, F. Mao and Z. Y. Zeng, *J. Power Sources*, **179**, 395 (2008).
20. R. J. Wen, Z. H. Yang, X. Fan, Z. Tan and B. Yang, *Electrochim. Acta*, **83**, 376 (2012).
21. J. L. Yang, Y. F. Yuan, H. M. Wu, Y. Li, Y. B. Chen and S. Y. Guo, *Electrochim. Acta*, **55**, 7050 (2010).
22. X. Xie, Z. Yang, Z. Feng, Z. Zhang and J. Huang, *Electrochim. Acta*, **154**, 308 (2015).
23. L. Wan, S. Yan, J. Feng, Z. Yang, X. Fan, Z. Li and Z. Zou, *Colloids. Surf. A Physicochem. Eng. Asp.*, **396**, 46 (2012).
24. Y. T. Prabhu, K. V. Rao, V. S. S. Kumar and B. S. Kumari, *Adv. Nanoparticles*, **2**, 45 (2013).
25. R. Marsalek, *APCBEE Procedia*, **9**, 13 (2014).
26. Y. F. Yuan, J. P. Tu, H. M. Wu, C. Q. Zhang, S. F. Wang and X. B. Zhao, *J. Power Sources*, **165**, 905 (2007).

27. H. Huang, L. Zhang, W. K. Zhang, Y. P. Gan and H. Shao, *J. Power Sources*, **184**, 663 (2008).
28. A. Ramadoss and S. J. Kim, *Mater. Chem. Phys*., **140**, 405 (2013).
29. J. Lee, P. Kumar, J. Lee, B. M. Moudgil and R. K. Singh, *J. Alloys Compd*., **550**, 536 (2013).
30. J. H. Lee, J. H. Chae, S. J. Kim, D. Y. Kim, N. K. Park and M. Kang, *J. Ind. Eng. Chem*., **16**, 185 (2010).
31. L. Neveux, D. Chiche, D. B. Bachi, L. Favergeon and M. Pijolat, *Chem. Eng. J*., **181-182**, 508 (2012).
32. M. H. Jung and M. J. Chu, *J. Mater. Chem. C*, **2**, 6675 (2014).
33. Y. F. Yuan, J. P. Tu, H. M. Wu, Y. Z. Yang, D. Q. Shi and X. B. Zhao, *Electrochim. Acta*, **51**, 3632 (2006).